Journal of Advanced Ceramics
2023, **12**(2): 207–227
https://doi.org/10.26599/JAC.2023.9220694
ISSN 2226-4108
CN 10-1154/TQ

Review

Metal oxide semiconductor gas sensing materials for early lung cancer diagnosis

Xiaoxi HE[a], Hongfeng CHAI[a], Yifan LUO[a,c], Lingfeng MIN[b], Marc DEBLIQUY[c], Chao ZHANG[a,*]

[a]*School of Mechanical Engineering, Yangzhou University, Yangzhou 225127, China*
[b]*Department of Respiratory and Critical Care Medicine, Northern Jiangsu People's Hospital Affiliated to Yangzhou University, Yangzhou 225001, China*
[c]*Service de Science des Matériaux, Faculté Polytechnique, Université de Mons, Mons 7000, Belgium*

Received: July 26, 2022; Revised: November 3, 2022; Accepted: November 7, 2022

Abstract: The urgency of early lung cancer (LC) diagnosis and treatment has been more and more significant. Exhaled breath analysis using gas sensors is a promising way to find out if someone has LC due to its low-cost, non-invasive, and real-time monitoring compared with traditional invasive diagnostic techniques. Among sensor-based gas detection techniques, metal oxide semiconductor's gas sensors are one of the most important types. This review presents the-state-of-art in metal oxide gas sensors for the diagnosis of early LC. First, the exhaled breath biomarkers are described with emphasis on the concentration of abnormal volatile organic compounds (VOCs) caused by the metabolic process of LC cells. Then, the research status of metal oxide gas sensors in LC diagnosis is summarized. The sensing performance and enhancement strategy of biomarkers provided by metal oxide semiconductor materials are reviewed. Another effective way to improve VOC detection performance is to build a gas sensor array. At the same time, various gas sensors combined with self-powered techniques are mentioned to display a broad development prospect in breath diagnosis. Finally, metal oxide gas sensor-based LC diagnosis is prospected.

Keywords: gas sensors; metal oxides; exhaled breath analysis; lung cancer (LC) diagnosis

1 Introduction

Lung cancer (LC) is one of the most frequent and deadly types of cancers [1–3]. According to the statistics collected in 2020, there were about 14 million new cancer patients, including about 2.2 million of LC. At the same time, around 1.8 million patients died from LC, which is 28% of all cancer deaths over the world. In recent decades, the incidence rate and mortality of LC have risen [4,5]. Although significant efforts have been made worldwide in early LC diagnosis, a large number of patients (over 60%) have missed the best opportunity for treatment, and their five-year survival rate is under 15%. If the patients are treated in time, their five-year survival rate can be

* Corresponding author.
E-mail: zhangc@yzu.edu.cn, zhangchao_cqu@hotmail.com

significantly increased, which indicated the significance and urgency of early LC screening [6]. Breath-analysis-based LC diagnostic techniques have recently attracted the attention of Khatoon *et al*. [7] and Mirzaei *et al*. [8]. Early research suggests that the concentration change of unique volatile organic compounds (VOCs) could be found in LC patients' exhaled gases, revealing that specific VOCs can be used as biomarkers for the early diagnosis of LC. Pauling *et al*. [9] put forward the idea of diagnosing the early state of LC by analyzing the exhaled gases of humans in the 1990s and found more than a dozen of VOCs related to it. Reference [10] also pointed out that about 250 VOCs in exhaled breath, existing at parts per million (ppm)/parts per billion (ppb) levels, could be used for LC diagnosis.

LC in the early stage has only inconspicuous symptoms such as fever and dry cough, which are easily ignored. This can cause a big trouble for the early diagnosis [11]. Traditional LC diagnosis based on approaches such as imaging examination, histopathological examination, and detection of tumor markers in body fluids have some disadvantages, including high cost and potential risk of health [12–14]. The existing respiratory diagnosis studies are mostly based on gas chromatograph–mass spectrometry (GC–MS), ion mobility spectrometry (IMS), or proton transfer reaction spectrometry (PTRS). Although these methods can give accurate information about low-concentration gases, they require large instruments with high cost and professional operators. Besides, it cannot provide real-time analysis, which limits the application in large-scale diagnosis of early LC [15]. Numerous gas sensors and sensor arrays have been developed for low-concentration gas detection in recent years, including surface acoustic wave (SAW) sensors and quartz crystal microbalance (QCM) sensors.

Generally speaking, exhaled breath consists of VOCs with concentrations from parts per trillion (ppt) to ppm level. Different biochemical and physiological mechanisms in the human organ produce the exhaled VOCs. As introduced in Ref. [16], the concentrations and components of VOCs in the human body will change when LC cells appear. Table 1 lists the relationship between partial VOC concentration and LC. For example, n-propanol, which is not found in a healthy subject, shows up in LC patient body [17–21]. The concentrations of toluene, o-xylene, and cyclohexane in patients were slightly higher than those of healthy subjects, while methanol had a relatively low concentration in LC patients [22–24]. Oxidative stress and the upregulation of cytochrome enzymes are directly linked to the emergence and progression of LC [25]. An excessive amount of reactive oxygen species (ROS) in the human body can cause damage to the cellular structure, which includes things like protein and polyunsaturated fatty acids. The process of oxidative stress can cause lipid peroxidation, which can in turn lead to a change in VOCs, so it is possible that oxidative stress is one of the factors [26]. These VOCs are excreted through exhaled breath [27]. Warburg effect is another possible source of VOCs, corresponding to the glycolysis that is activated in hypoxic conditions over oxidative phosphorylation. This reaction produces an excess of lactic acid that may eventually result in the formation of trace VOCs. Figure 1 summarizes the theory of how different kinds of VOCs are generated in the body of early LC patients.

Metal oxide semiconductors enable the development of low-cost, miniature, and high-performance sensors for VOC analysis in exhaled breath. They are free of collateral damage, respond quickly, and have relatively high response. The use of gas sensors based on metal oxide semiconductors will aid in the development of an electronic nose (e-nose) system that is simple, convenient, and low-cost. It can monitor and analyze the composition and concentration changes of exhaled gases in real time and infer the metabolic and healthy status of the body from the abnormal VOCs level [15,26,32,36]. The e-nose systems can offer the fingerprint of VOCs and give a quantitative response. It is a very powerful LC diagnosis tool [26]. The gas-sensitive and selective property of the semiconductor gas sensor can be improved by modifying it with various advanced materials. As a result, it will be better able to analyze complex VOCs during the process of breathing, which will contribute to LC diagnosis [16].

Over the past few years, researchers have carried out numerous works to enhance gas sensing performance. However, there are still many challenges in the aspect of real-time breath detection due to the influence of high humidity and multiple interfering gases. Pretreatment processes such as dehumidification and filter are significant to improve the accuracy of breath diagnosis when the resistance property of metal oxide materials cannot meet the requirement. An ideal respiratory gas sensor should have excellent selectivity, moisture

Table 1 Gas concentrations of LC patients and healthy people

Biomarker	n-propanol [28]	Toluene [29]	Isoprene [30,31]	Cyclohexane [28]	Acetaldehyde [32]	Formaldehyde [33,34]	2-butanone [35]
Concentration for healthy subjects (ppb)	—	< 30	< 12	25	5	48	0.45–2.34[a]
Concentration for sick patients (ppb)	450	> 30	12–580	200	100	83	0.79–4.25[a]

[a]The units of the data are nmol/L.

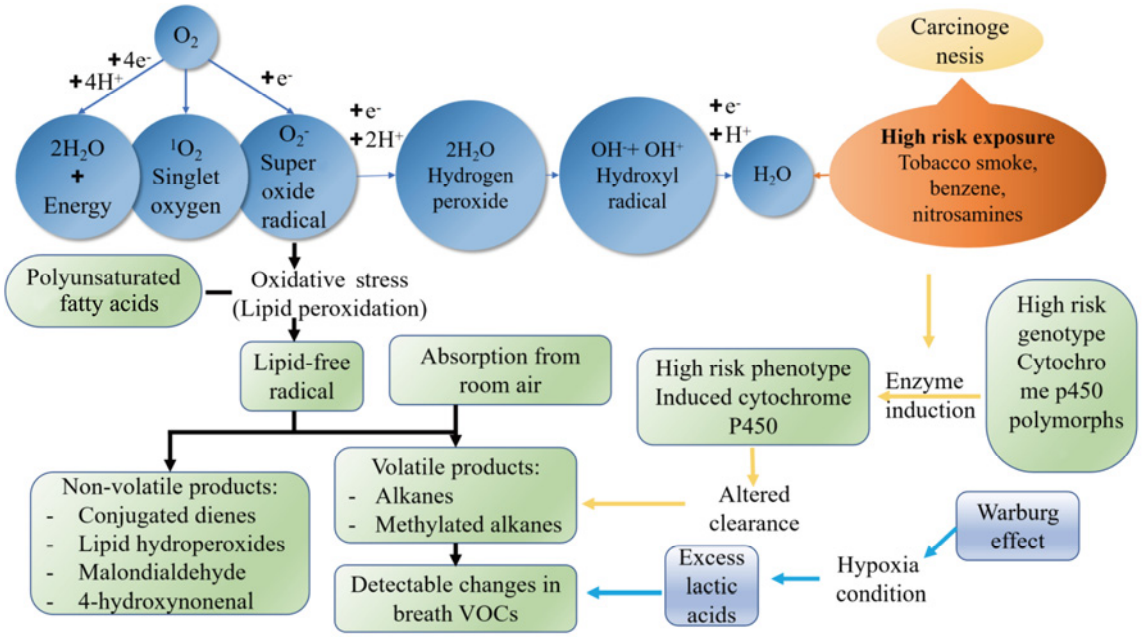

Fig. 1 Hypothetical basis of breath analysis technology for the detection of early LC.

resistance, ppb-level detection limit, and high sensitivity. Therefore, it is urgent to develop gas sensing materials with excellent performance to meet the requirements of LC respiratory diagnosis. This review covers the research progress of metal oxide gas sensing materials for different LC VOCs, integrated gas sensor arrays for LC diagnosis, and self-powered gas sensors for the breath analysis.

2 Metal oxide semiconductor gas sensors

As early as the 1960s, Seiyama *et al.* [17] successfully prepared a stable ZnO thin film for H_2 detection, establishing the foundation for the later application of metal oxide semiconductor gas sensor. In the 21st century, material science had accelerated the research and application of metal oxide gas sensors, and gradually entered the field of disease diagnosis. A small, low-cost, and fast e-nose made of six highly sensitive (ppb-level) metal oxide gas sensors (fabricated by SACMI S.C.) was built for early LC screening in 2007 [18]. Subsequently, studies on metal oxide-based LC-exhaled analysis have mushroomed, as described in Section 2.

2.1 Working mechanism

The respiratory analysis technique based on metal oxide gas sensors is a field with rapid development. Metal oxide gas sensors measure the conductivity change caused by the electron transfer between the sensitive material and the target gas during adsorption and reaction. The concentration change of charge carriers may be seen in the sensing layer, which is associated with the adsorption of gas molecules. As shown in Fig. 2, we take an n-type metal oxide semiconductor as an example to graphically display the mechanism. When exposed in air, oxygen atoms adsorb on the sensor surface. This causes the resistance to increase because the oxygen atoms take electrons from the metal oxide material to form adsorbed oxygen ions. The existing forms of adsorbed oxygen ions are related to the temperature (T). Generally, when T < 100 ℃, oxygen ions are in the form of O_2^-; when

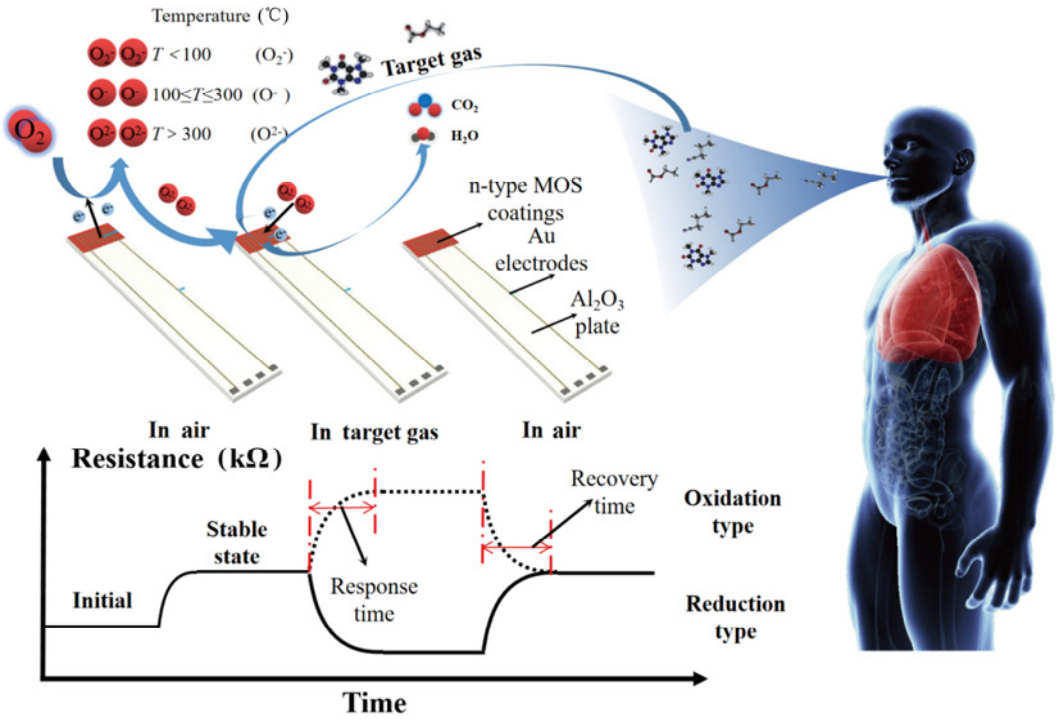

Fig. 2 Working mechanism of n-type metal oxide gas sensors for LC detection.

100 ℃ ⩽ T ⩽ 300 ℃, oxygen ions mainly exist as O^-; when T > 300 ℃, the oxygen ions are mainly O^{2-}. Adsorbed oxygen forms an electron depletion layer on the sensitive material's superficial layer, increasing the potential barrier at the grain boundary and the material's resistance [19]. When oxygen ions react with a reducing gas, they restore the acquired electrons to the metal oxide. This reduces the gas sensor's resistance. When the target gas is an oxidizing gas, the sensing material's electrons are further depleted. The resistance change of the sensing layer is measured, which can reflect the gas information such as the type and concentration [20]. When used for LC analysis, the disease is determined by analyzing the data from metal oxide gas sensor-based e-nose.

2. 2 Sensing materials

In order to accurately exhibit the exhalation information and give the correct detecting results, it is necessary to fabricate a sensitive layer with high sensing performance to target gases. Most metal oxide semiconductors can be applied as semiconductor gas sensors. Metal oxide is a compound formed by oxygen and one or more metal elements in one phase. It can be divided into binary, ternary, and multicomponent metal oxides and hybrid materials (such as carbon nanotube (CNT)–metal oxide, graphene–metal oxide, MXene–metal oxide, and organic material–metal oxide).

An obstacle to applying metal oxide semiconductors to breath analysis is the lack of selectivity among different VOCs, especially for the VOCs in the same family. For example, most e-nose systems use commercial metal oxide sensors, which lack selectivity, resulting in the demand for adding different sensors [21,22,26]. The metal oxide gas sensor's sensitivity could be boosted by the addition of a noble metal according to Refs. [23,24,37–39]. Doping strengthens the gas sensor sensing performance by modifying the bandgap structure and decreasing charge carriers' activation energy. Morphology controlling, recombining, and introducing high-concentration defects also showed remarkable enhancement to their kinetics [40–42].

2.2.1 Binary metal oxide

Binary metal oxide semiconductors refer to the oxide phase composed of one kind of metal atom, and it is usually segmented into type n and p based on the charge carriers. Common n-type metal oxides include ZnO, SnO_2, WO_3, α-Fe_2O_3, and CeO_2, while p-type metal oxides include Co_3O_4, NiO, CuO, and Mn_3O_4 [30,43,44]. The binary metal oxide is the metal oxide gas sensing material that has been mainly studied. The

concentrations of VOCs in exhaled breath are generally low, mainly existing in ppb level, and the complex compositions of exhaled breath bring a large number of interference gases, which affect the sensing result of metal oxide gas sensors. As a result, the high detection limit and poor selectivity of pure binary metal oxide sensing materials can no longer meet the demand. Güntner *et al*. [33] prepared highly porous SnO_2 films doped with Pt, Si, Pd, and Ti by flame spray pyrolysis (FSP). Pt, Si, Ti, and Pd are chosen as dopants to induce different analyte selectivity among the sensors. It could achieve a stable response under the relative humidity (RH) of respiratory gas (about 90%). The e-nose based on SnO_2 gas sensors for LC diagnosis had good detection performance, which could achieve accuracy and sensitivity of over 80% [45–47]. However, the array needs to work at a high temperature, which is a waste of energy and a challenge to the service life of the sensor. A series of methods (doping, surface modification, structure and morphology control, compounding, and photocatalysis) have been used to strengthen the binary metal oxide gas sensing properties, such as porous SnO_2 hollow spheres [23], Pt-decorated indium oxide (In_2O_3) nanoparticles [24], flower-like WO_3/In_2O_3 hollow spheres [37], ZnO with surface oxygen vacancies [38], and self-assembled WO_3 nanowires [39].

2.2.2 *Ternary and multi-element metal oxides*

Ternary and multi-element metal oxides refer to one phase composed of two or more metal elements. It has the advantages of binary metal oxide and some other advantages such as abundant multivalent cations, unique crystal structures, and controllable compositions, which means that this gas-sensitive material has great potential. The research of multi-element metal oxide semiconductor sensitive materials focused more on doping, synthesizing porous structures, and the proportion of metal elements [48]. Lai *et al*. [29] synthesized $NiFe_2O_4$ with an ordered mesoporous framework structure by taking mesoporous SiO_2 (KIT-6) as a template. The ultrathin mesoporous $NiFe_2O_4$ material had a large specific surface area (SSA) of up to 216 $m^2 \cdot g^{-1}$, which brought the excellent response and low limit of detection to toluene (a possible LC biomarker). Besides, noble metals were loaded upon the surface of $ZnFe_2O_4$ to improve potential gas sensing properties, which could be explained by p–n junctions formed between metal ions and matrix materials [49,50]. The existence of p–n heterojunction generated Schottky barrier at the interface and resulted in a synergistic gas sensing effect, as shown in Fig. 4(e). In other directions, materials such as $CaFe_2O_4$–$ZnFe_2O_4$ and perovskite-type $La_{0.8}Pb_{0.1}Ca_{0.1}Fe_{0.8}Co_{0.2}O_3$ were used for enhancing gas sensing properties [51,52]. Although these methods or materials had not been directly used for LC detection, they were of guiding significance for developing ternary or multi-element metal oxide-based exhaled breath analysis.

2.2.3 *Hybrid materials*

The research of metal oxide semiconductor sensing materials should not limit to utilize a single type of material. Hybrid materials include CNT–metal oxide, graphene–metal oxide, MXene–metal oxide, and organic material–metal oxide. When various semiconductors are combined, heterojunctions typically form at the interface as a result of different work functions of the constituent semiconductors. As a result, the concentration of free charge carriers at the interface improves gas sensing performance.

1) CNT and graphene composites

In recent years, researchers have been particularly interested in one-dimensional (1D) and two-dimensional (2D) carbon materials due to unusual structural and electronic properties. CNTs show unique conductivity and long-term stability due to the nanometer diameter, the large SSA, and the unique conjugation effect of carbon atoms. It gives CNT-based materials good detection ability at room temperature and potential medical diagnosis application [53–56]. Inaba *et al*. [57] deposited p-type CNTs and n-type SnO_2 on SiO_2 ceramic substrate by one-step dielectrophoretic assembly technology to form a composite sensing material with heterojunction. This study pointed out that different mixing ratios of CNTs and SnO_2 greatly influence their gas sensing performance. The composition of the two materials would form an electron depletion layer at the interface of CNT/SnO_2 heterojunction, resulting in a high response. Graphene is a 2D layered structure material with good flexibility, and the unique structure could shield the charge fluctuation well [58]. However, pure graphene is chemically inert and difficult for the target gas to attach to its surface, which limit its gas sensing performance. It is usually used together with metal oxides to make hybrid materials with heterostructure [59].

2) MXene composites

MXene is a 2D layered material discovered by Gogotsi in 2011, which is generally in the form of $M_{n+1}X_n$. M represents an early transition metal, and the X represents carbon or nitrogen. It has various advantages, including outstanding mechanical strength, affluent active sites, large SSA, rich electron density, adjustable structural crystallinity, and chemical durability. MXene is prepared by selective etching in acidic solution. Its unique physical, chemical, and structural characteristics attract much attention and open up new prospects for MXene out of energy storage and conversion [60–64]. References [32,65,66] indicate that MXene-based 2D materials offer various merits for precisely detecting various breath biomarkers. Many researchers are hammering at realizing MXene as VOC sensing materials. Among the vanguardist, CuO and MXene hybrid nanocomposites were successfully synthesized by electrostatic self-assembly, in which CuO was evenly distributed on the surface and middle layer of multilayer accordion-like MXene. On account of the formation of hybrid heterostructures, the composites exhibit better gas sensing properties to toluene than pure CuO and MXene materials [67].

3) Organic semiconductor composites

Generally, organic semiconductor materials can be divided into small organic molecular materials (mainly containing porphyrin, porphin, and metal phthalocyanine complexes) and conductive polymer materials (mainly containing polypyrrole, polythiophene, and polyaniline (PANI)). The molecular diversity and functional groups of organic materials give them excellent selectivity to target gas as well as low response and high detection limit due to low working temperatures. To improve the sensing performance of a single kind of organic or inorganic materials, Umar *et al*. [68] and Duan *et al*. [69] thought of compounding organic and inorganic materials with complementary properties, hoping to prepare gas-sensitive materials with excellent properties. Ni-doped SnO_2 and polythiophene nanocomposites prepared by oxidative polymerization had proved to have better properties to NO_2 than homogeneous materials. Bai *et al*. [70] prepared the composite gas sensing materials of PANI and SnO_2 by simple oxidative polymerization. At room temperature, this substance exhibited a high level of sensitivity, excellent selectivity, and an expansive linear response range. The main reasons for the sensing performance enhancement were the complementary synergistic effect between SnO_2 and PANI and the formation of p–n heterojunction upon the interface.

3 Sensors for LC biomarker detection

3.1 Metal oxide semiconductor materials for different LC VOCs

Metal oxide gas sensors specially used for detecting specific VOCs related to LC have great potential in e-nose application. They can ease data processing and be patient-friendly as a result of short response and specific selectivity. We counted the types of VOCs mentioned in relevant studies and selected some of the most frequently mentioned VOCs as cases (propanol, toluene, 2-butanone, formaldehyde, etc.). We summarize some proposed sensors for LC biomarker gas detection to guide the selection or production of sensors in relevant e-nose systems.

3.1.1 Propanol

n-propanol and isopropanol are both recognized as important VOCs for early LC diagnosis [28,71]. In the growth process of LC, cells will create non-essential n-propanol in the body. Excess n-propanol is removed from the body via fluid and exhaled breath. The n-propanol concentration is zero in a healthy body, while that of LC patients may exceed 450 ppb [28]. Hence, abnormal n-propanol concentration could indicate potential LC. It is quite essential to fabricate gas sensors that can effectively monitor the concentration of propanol for the early diagnosis of LC, which should meet some requirements like short response (< 10 s), good selectivity, excellent response, and low detection limit [72]. Various nanocomposites based on metal oxide semiconductors have been extensively researched to achieve high sensitivity and fast response, such as Fe-doped ZnO [13,73], 5% Ag-modified hollow sphere In_2O_3 [42], Cu-doped In_2O_3 [74], ZnO nanoparticles [75], double-shell Cu_2O hollow microspheres [76], $ZnSnO_3$ [77], NiO [78], and ZnO–NiO [79]. Figure 3 displays the sensing performance of propanol sensors based on different metal oxide semiconductors [13,76,79], proving a sufficient sensitivity for breath propanol detection. For example, Wang *et al*. [76] used a solvothermal technique to create double-shell Cu_2O hollow microspheres. Figures 3(c) and 3(d) indicate that the double-shell material exhibits regular response between 10 and 100 ppm. The linear

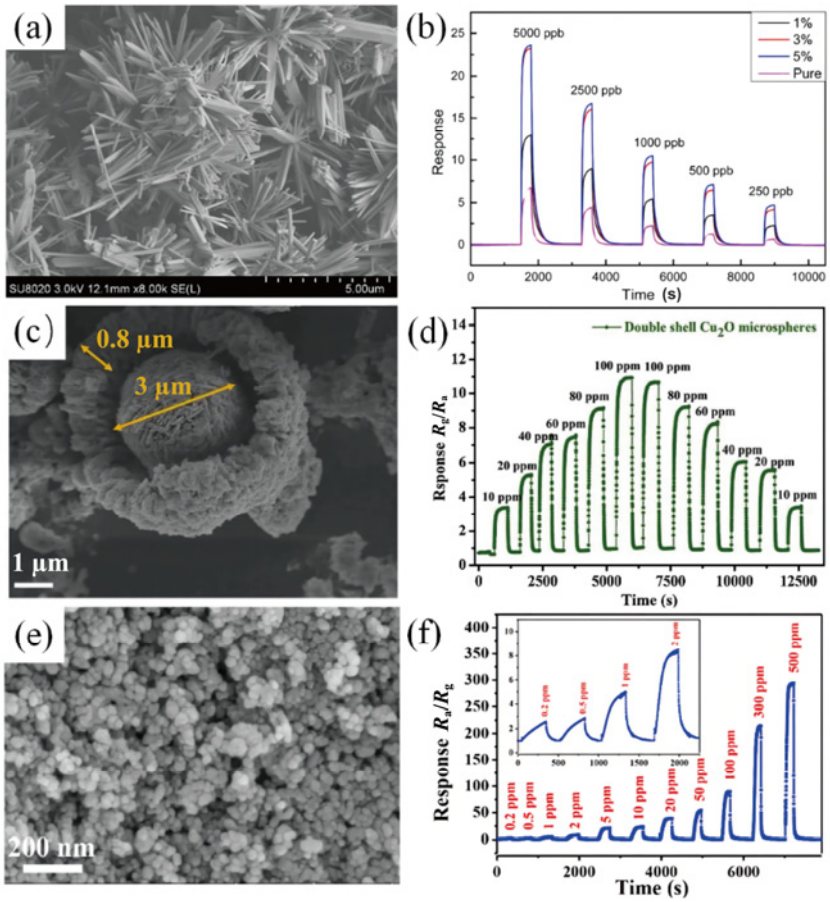

Fig. 3 (a) Scanning electron microscopy (SEM) image of pure ZnO nanoneedles and (b) response of pure and Fe-doped ZnO nanoneedles to isopropanol with 50% of humidity at 275 ℃. (c) SEM image of double-shell Cu_2O hollow microspheres. (d) Dynamic response of sensors based on double-shell Cu_2O hollow microspheres. (e) SEM image of ZnO/NiO-48 h surface. (f) Dynamic response of ZnO/NiO-48 h sensor for various n-propanol concentrations (0.2–500 ppm) at 275 ℃. Reproduced with permission from Ref. [13] for (a, b), © Springer Science+Business Media, LLC, part of Springer Nature 2020; Ref. [76] for (c, d), © Elsevier B.V. 2021; Ref. [79] for (e, f), © American Chemical Society 2021.

relationship between response and n-propanol concentration was 0.9835. Furthermore, the optimal operating temperature for the sensor was determined to be 187 ℃ after analyzing the effects of various temperatures on the sensor response, and it was also found that the double-shell Cu_2O showed better selectivity to n-propanol at 187 ℃. There was very little gas reaction with adsorbed oxygen on the surface at temperatures lower than the optimal working temperatures. The preparation of a double-shell structure can increase the speed of response and recovery. The shell layers of the prepared double-shell hollow sphere are loose and porous and exist enough gaps between the shell layers, making a great SSA. When the distance between the interlayer channels is larger, there is more room for more gas molecules to spread into it, which results in more active reaction sites on the interior of the structure.

In the past few years, metal-ion catalysts have proved to offer opportunities in many important fields. Due to their unique electronic and chemical properties, the application of metal ions in gas-sensitive materials provides high activity and special selectivity for the adsorption of gases and electron transport [80]. Luo *et al*. [13] found that Fe-doped ZnO nanoneedle materials synthesized by a hydrothermal method had an excellent response to isopropanol for concentrations of lower than 5 ppm. ZnO is a qualified metal oxide for breath analysis among all those materials. The effect of different Fe doping contents on isopropanol was studied by Luo *et al*. [13]. When the sensor surface contacted isopropanol, the sensor resistance was significantly reduced, probing that the Fe-doped ZnO material maintains n-type. Under certain circumstances, the sensitivity of the sensors to the presence of isopropanol rises in proportion to the amount of present iron [73]. When the maximum

content of Fe was 5%, the RH was 50%, and the optimal temperature was 275 ℃, the response to 250 ppb isopropanol could be equal to 4.7 and reach a stable state within 51 s. Fe-doped ZnO improved the response and selectivity to isopropanol, reduced the working temperature, and maintained stability in the range of high RHs. Besides, it also showed excellent long-term stability that only a small offset occurred in the test after 10 d. In general, the decoration of metal oxides with noble metals is able to significantly improve the performance. Besides, Zhang *et al*. [42] considered loading noble metal ions on hollow sphere In_2O_3 surface. In the end, they concluded that Ag offered the balance between cost and performance. 5 at% Ag-modified hollow sphere In_2O_3 could exhibit the highest possible sensitivity to isopropanol at 300 ℃. Its response to 5 ppm isopropanol is 5.2, whereas the response of a pure In_2O_3 sensor is 0.8. This indicates that its response to 5 ppm isopropanol is approximately 6.5 times higher than that of the pure In_2O_3 sensor, and its response to 200 ppb isopropanol is 0.6. Compared with those of other studies with the detection limit of > 10 ppm, this material (Ag–In_2O_3) shows good sensing characteristics to isopropanol at low concentrations. Cu-doped In_2O_3 hollow nanofibers also proved to play great gas sensing performance [74].

A ZnO nanoparticle-based sensor prepared by Kortidis *et al*. [75] could react well with n-propanol due to more –CH_2– groups, relatively high oxygen vacancies, and doubly ionized oxygen vacancy concentrations [81]. It was prepared by a hydrothermal method with zinc nitrate and sodium hydroxide in a reactor for 4 h. The response of this sensor was significantly influenced by the working temperature [82,83]. Tests showed a maximum response of 6.6 towards 40 ppm n-propanol at 125 ℃. After 190 s of contact with n-propanol, the current began to rise steadily. In various gas comparison tests, the sensor showed a higher response to n-propanol. ZnO-4 h-based sensors still showed very stable performance after 45 d. By investigating the influence of hydrothermal time on sensor response, it was found that long-time hydrothermal led to the reduction of sensor response, which may be due to the reduction of oxygen vacancy concentration.

Due to the unique cubic octahedral molecular space structure of ternary metal oxide $ZnSnO_3$, more oxygen vacancies increase the adsorption sites and promote their gas-sensitive performance. The $ZnSnO_3$ sensor strengthened by Yin *et al*. [77] met the expectation, where the sensor revealed a response of 1.7–500 ppb of n-propanol at 200 ℃. Furthermore, the sensor worked well with n-propanol at different concentrations and temperatures up to 100 ℃. A simple co-precipitation approach was used to produce $ZnSnO_3$ nanospheres composed of multiple thin triangular nanosheets. Zn, Sn, and O elements were uniformly distributed in triangular nanosheets. The results are exhibited in Figs. 4(a)–4(c).

NiO, a p-type semiconductor material that has not been widely concerned, could further reduce the working temperature. According to Mokoena *et al*. [78], NiO, generated from urea and calcined at 400 ℃, has an extremely large SSA (the maximum value = 294 $m^2 \cdot g^{-1}$) and perfect crystallinity. They brought more adsorption sites, and the improved crystallinity could promote the mobility of charge carriers, which were conducive to the gas-sensitive process. This sensor had a high sensitivity of 1.59, a low detection limit of 20 ppb, and a good selectivity to the target gas at 75 ℃. When the working temperature was raised to 100 ℃, the response speed became faster, and it appeared a linear relationship existed between reaction and concentration. NiO thin film showed incredible linearity in a wide concentration range and ppb-level detection limit on account of the mutual effect of large SSA with –OH functional group of n-propanol. Zhao *et al*. [79] considered that bimetallic organic frameworks were one of the most ideal precursors to product metal oxide materials. They successfully fabricated ZnO/NiO heterostructure from Zn/Ni bimetallic organic frameworks. ZnO/NiO exhibited a significant response of 2.51–200 ppb n-propanol (the low detection limit) at 275 ℃ (Figs. 3(e) and 3(f)). The synergistic effect of the heterojunction between the interface of ZnO and NiO nanoparticles and the chemical sensitization effect of NiO could explain the enhanced performance of the sensor for n-propanol. ZnO is a well-known n-type semiconductor, whose charge carrier is electrons, whereas NiO is a p-type semiconductor with holes as the charge carriers. Due to the lower Fermi energy level of NiO, the holes will flow from NiO to ZnO when the two substances come into contact with one another, whereas the electrons will transfer in the opposite manner [84]. This phenomenon makes the resistance of the sensor higher in air and lower in n-propanol gas, resulting in more significant response. In conclusion, experiments and theories sustain the

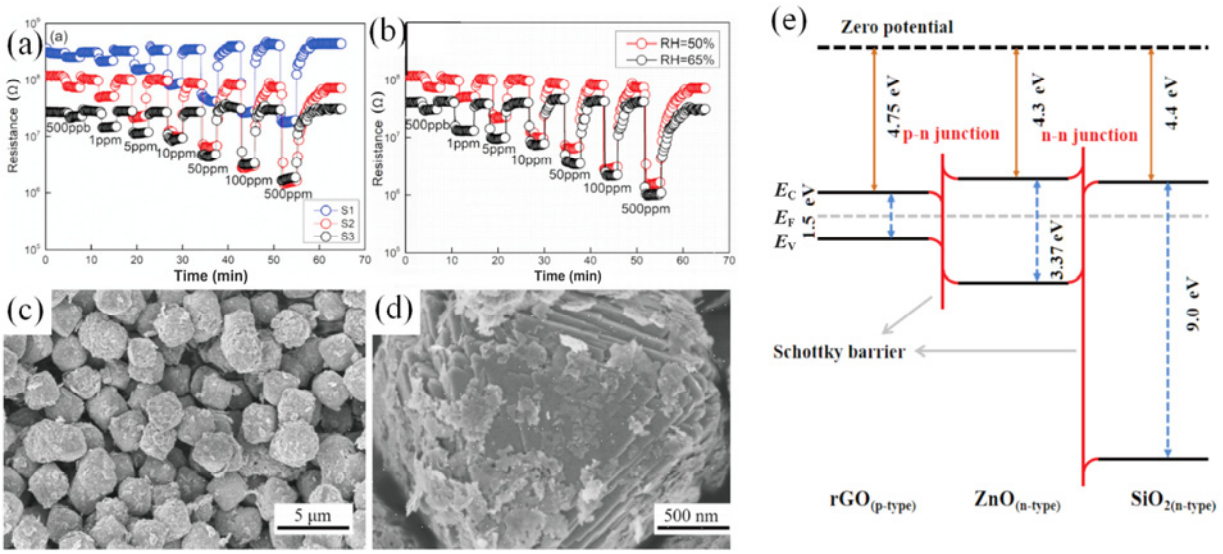

Fig. 4 (a) Response–recovery curves of three sensors to n-propanol gas with different concentrations. (b) Response–recovery curves of S2 $ZnSnO_3$ sensor upon exposure to n-propanol gas with different concentrations under RH = 50% and 65% at 200 ℃. (c, d) Low-magnification and high-magnification SEM images of $ZnSnO_3$ nanospheres, respectively. (e) Energy band diagram of ZnO@SiO_2/reduced graphene oxide (rGO) nanocomposite in target gas. Note: E_C, E_F, and E_V represent the energy of the conduction band, the Fermi level, and the valence band, respectively. Reproduced with permission from Ref. [77] for (a–d), © Elsevier B.V. 2020; Ref. [41] for (e), © Elsevier B.V. 2021.

prospect of metal oxide gas sensor sensing n-propanol biomarkers.

3.1.2 Toluene

Toluene is supposed as a very important potential VOC biomarker for early LC diagnosis. Its concentration in exhaled breath of healthy people should not exceed 70 ppb [29,85,86]. Toluene's reaction pattern in LC breath analysis utilizing metal oxide gas sensors is a non-target strategy because smoking causes similar response. Some common VOC pollutants in air may interfere with the response of toluene gas sensor, and hence it is important to make metal oxide gas sensor materials with excellent sensing properties.

Metal oxide semiconductor materials also exhibit excellent sensing performance toward toluene. Especially, ppb-level detection of toluene can be achieved by SnO_2 with different nanostructures (e.g., porous cubic octahedral egg yolk–shell SnO_2 [87], three-layer hollow cubic SnO_2 [88], and single-layer hollow cubic SnO_2 [89]). Bing *et al*. [87] fabricated a multi-layered structure of porous cubic octahedral egg yolk–shell SnO_2 sensor through a simple annealing and etching strategy, as exhibited in Figs. 5(a)–5(d). Besides, as shown in Fig. 5(e), the fabricated sensor could respond to 20 ppm toluene and exhibit a short response time of 1.8 s at 250 ℃. It is mainly due to the fact that particles were less agglomerated and had sufficient clearance leaving between different shells, which can be used as buffer space in the process of gas induction. Compared with traditional solid spherical granular materials, the porous multi-wall materials composed of different-sized pores had larger SSA and richer adsorption sites. From the characterization results, it could be seen that the particles exist in the form of face-to-face contact, which showed wider electron channels between adjacent particles and reduces the height of the Schottky barrier, thus achieving high response and rapid recovery. As a kind of low aggregation structure, hollow nanostructure had the characteristics of low density, large SSA, and strong adsorption capacity. By changing the particle size and morphology, a reasonable design of a low agglomeration hollow structure could bring good performance. Based on the double-shell structure, Wang *et al*. [88] prepared three-layer hollow cubic SnO_2 by a low-cost and multi-step method (Fig. 5(f)). Its SSA was 122.7 $m^2 \cdot g^{-1}$, and its average pore diameter was 7.2 nm. The three-layer hollow cubic SnO_2 showed high response of 20–38.7 ppm toluene at 250 ℃, which was significantly higher than single-layer and double-layer structures. At the same time, the response time was less than 1 s, which could almost achieve an instantaneous response. This excellent sensing characteristic may be related to the structural robustness of the three-shell structure and

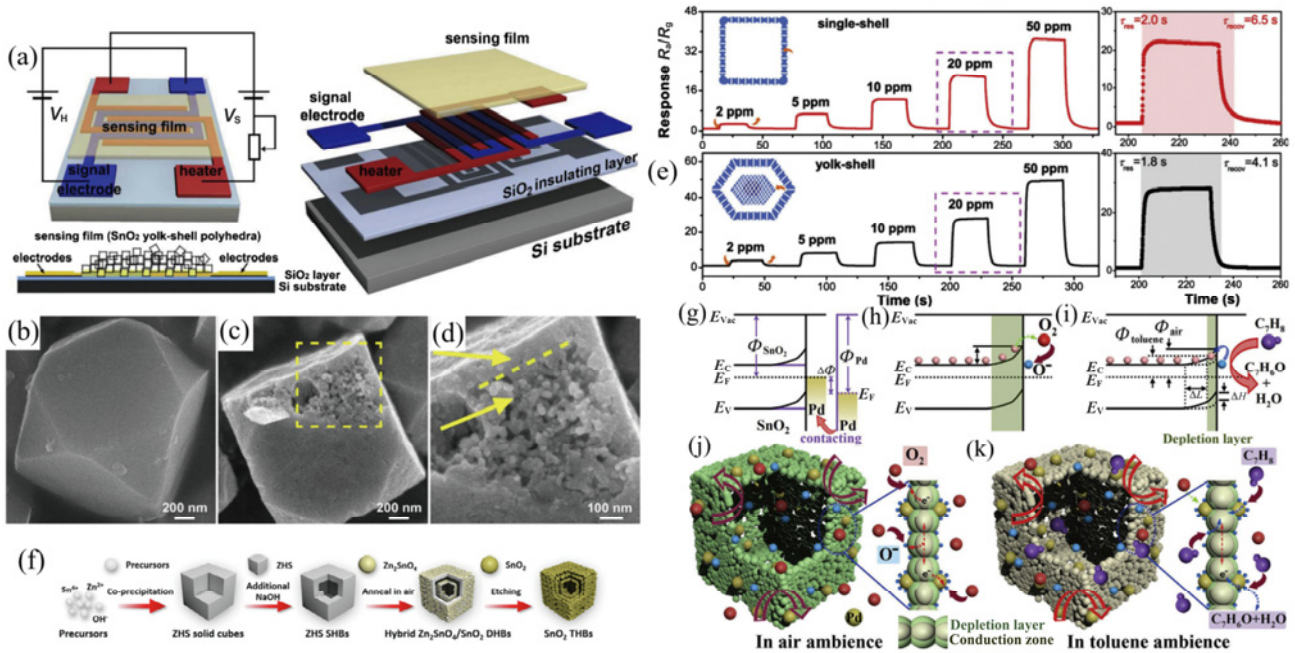

Fig. 5 (a) Schematic diagrams with different perspectives showing the sensor structure based on SnO_2 products. (b–d) Typical field-emission SEM (FESEM) images of Zn_2SnO_4/SnO_2 cuboctahedron. (e) Dynamic toluene sensing transients of SnO_2 products with single-shell structures and yolk–shell structures to toluene with different concentrations. (f) Schematic illustration of the overall process for SnO_2 THBs. Schematic energy band diagrams of SnO_2 and Pd contact (g) with establishing the contact and with being exposed to (h) air and (i) toluene ambience. (j, k) Schematic diagrams of possible gas sensing mechanisms of Pd-loaded SnO_2 porous cages. Reproduced with permission from Ref. [87] for (a–e), © Elsevier B.V. 2016; Ref. [88] for (f), © Elsevier B.V. 2020; Ref. [89] for (g–k), © Elsevier B.V. 2016.

various activated surfaces, which was very attractive for gas sensors. The enhancement strategy of increasing the SSA by preparing multilayer shells enhanced the adsorption and desorption rates of toluene and realized a rapid response. However, it was still far from the required detection limit.

By adding Pd on SnO_2, Qiao *et al*. [89] showed that a low detection limit of 100 ppb for toluene can be reached. At 230 ℃, the response of a single-layer hollow cubic SnO_2 structure loaded with Pd to 20 ppm toluene was slightly higher than that of Wang *et al*.'s three-shell hollow cubic structure [88], and the response time was further shortened. Compared with the large SSA of 122.7 $m^2 \cdot g^{-1}$ of the three shell layers, the SSA of the single-layer structure loaded with Pd was only half of it. However, it still had similar gas-sensitive performance, which showed that the catalytic effect of noble metal particles can improve the gas sensitivity of metal oxide materials more conveniently. The enhanced catalytic activity of Pd-loaded for oxygen dissociation improved the conversion rate of molecule ions and the number of adsorbed oxygen ions, resulting in a faster electron depletion rate of Pd-loaded SnO_2 and improved sensing reaction and performance. Figures 5(g)–5(k) show these results. The larger the SSA is, the faster the recovery can reach.

In order to further improve the gas sensitivity to toluene, researchers have tried to explore other sensitive materials with excellent sensing properties. Lai *et al*. [29] proposed to synthesize $NiFe_2O_4$ with an ultra-thin ordered mesoporous framework structure using mesoporous SnO_2 (KIT-6) as a template. Prior to this, there was little research on mesoporous $NiFe_2O_4$, and there was no research on the application of this material in gas sensors. The material had an SSA of up to 216 $m^2 \cdot g^{-1}$. By changing the hydrothermal temperature in the preparation process, the pore size could be reduced to 5.6 nm, and the thickness of framework could be reduced to 5 nm. Compared to bulk granular materials, the ultra-large SSA, small mesoporous size, and ultra-thin skeleton brought the gas response of 1–77.3 ppm toluene and could detect 2 ppb at 230 ℃. According to the research report, this may be related to the fact that $NiFe_2O_4$ is a p-type metal oxide material. Compared with most widely studied n-type metal oxide materials, p-type materials had a better catalytic effect on toluene gas, and humidity had less influence on sensitivity. This work

offered a significant chance for realizing $NiFe_2O_4$ as selective toluene detection in breath analysis, because its detection capability was potentially competitive with those existing respiratory diagnostic techniques.

3.1.3 2-butanone

2-butanone is a vital VOC biomarker of LC [90]. It was detected in the exhaled breath of LC patients, possibly due to the increased fatty acid oxidation during cancer progression. Besides, significantly higher alcohol dehydrogenase activity has been observed in many cancer cells, which oxidizes secondary alcohols and contributes to 2-butanone production [91]. Therefore, the detection of 2-butanone is essential for the non-invasive LC diagnosis. According to Fu *et al*. [35] and Buszewski *et al*. [92], the concentration of 2-butanone in the human body is very low, and there is a cross concentration interval. Numerous butanone-sensing materials based on metal oxide semiconductor have been investigated, including bicone-like ZnO [93], Ce-doped SnO_2 [94,95], three-dimensional (3D) urchin-like WO_3 [96], and Zn_2SnO_4 nano cubes [97].

Ce is a rare-earth element with different valences of Ce^{3+} and Ce^{4+}, which can quickly migrate oxygen ions and has good catalytic performance. Zhang *et al*. [94] made Ce-doped SnO_2 using an eco-friendly hydrothermal method. The crystal structure of SnO_2 was altered by the addition of Ce, which resulted in a significant increase in gas sensitivity. The catalytic effect of Ce made the surface of the SnO_2 have high chemical activity, and the activation energy of gas adsorption reaction was low. The detection limit reached 500 ppb, and the response to 20 ppm 2-butanone was 2.9 times that of pure SnO_2 in 20 s at 175 ℃. Moreover, the sensor response hardly changed in the long-term cycling test. Jiang *et al*. [95] had a similar idea to Zhang *et al*. [94]. Jiang *et al*. [95] used a simple sol–gel and dip-coating method to fabricate Ce-doped SnO_2 thin films. The doping of Ce made the grain size smaller. In the two studies, the optimum doping amount of Ce was 1 at%. Excessive doping had a negative impact on gas sensing performance. The excess Ce occupied the grain boundary of SnO_2 phase and hindered the carrier migration between it.

The research and development of mesoporous materials are of great significance for the gas sensing materials. The definition of mesoporous material is a kind of porous material, whose pore size is between 2 and 50 nm. This pore size is suitable for the gas molecules to pass through, which can increase the surface coverage of the gas molecules and improve the gas sensing performance. The mesoporous materials have various shapes, and the pore wall composition and properties can be controlled. It is also attractive because of its potential applications in catalysis, adsorption, separation, and optic, electric, magnetic, and other fields. Tian *et al*. [96] synthesized 3D urchin-like WO_3 with a mesoporous structure composed of interconnected nanorods through a simple hydrothermal method. The presence of mesoporous facilitated the spread of gas molecules. The 3D structure provided abundant active sites and nano-junctions, which promoted the adsorption of gas molecules, electron transfer, and adsorption/desorption rate. The response to 50 ppm 2-butanone was 188.5 at 240 ℃, and the detection limit could reach 100 ppb. Besides, sensor sensitivity had a good linear relationship (R^2 = 0.9765) in the concentration range of 0.1–50 ppm, showing its reliability for butanone detection (Figs. 6(a) and 6(b)). The response and recovery performance of the prepared WO_3 in detecting 5 ppm butanone are revealed in Fig. 6(c). Zhu *et al*. [98] synthesized Ag-modified porous spherical NiO material by the hydrothermal method (Figs. 6(d)–6(f)). The strategies of doping, morphology controlling, compositing, and other methods have positive effects on gas-sensitive butanone, which hold great potential in the diagnosis of LC.

3.1.4 Formaldehyde

Formaldehyde is a common toxic carcinogen in the environment and an important biomarker for LC [34,99]. LC patients have been shown to convert active aldehydes into stable oximes by means of on-fiber-derivatization (SPME-OFD) [100]. It was reported that the average concentration of formaldehyde in healthy people is 48 ppb, while the average concentration in LC patients is 83 ppb [34]. As one of the important biomarkers of LC VOCs, it has attracted more and more attention. The progress in fundamental research of metal oxide semiconductor nanomaterials has enabled significant development of high-performance formaldehyde sensors [101], such as rGO–SnO_2 [34], $LaFeO_3$ film [99], In-doped $LaFeO_3$ [102], Au/Pd-modified SnO_2 [103], Au–V_2O_5 [104], and ZnO–SnO_2 [105]. They could realize the sensitive detection of ppb-level formaldehyde under certain conditions (100–300 ℃). Especially, Hu *et al*. [99] and Yang

et al. [106] prepared multilayer porous $LaFeO_3$ by a simple sol–gel method as a high-performance formaldehyde gas-sensitive material. As shown in Figs. 7(a)–7(d), the $LaFeO_3$-based sensor exhibits

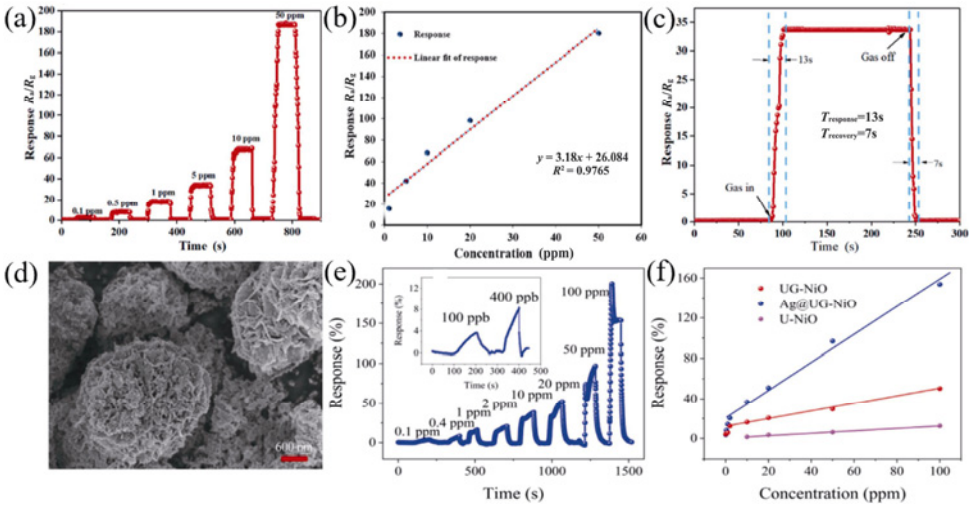

Fig. 6 (a) Response toward 2-butanone with different concentrations of 0.1–50 ppm measured at 240 ℃. (b) Linear relationship between gas sensitivity and gas concentration. (c) Response/recovery time toward 2-butanone with 5 ppm at 240 ℃. (d) SEM image of 3.9% Ag@UG–NiO. (e) Response of 3.9% Ag@UG–NiO to different concentrations of butanone. (f) Linear fitting of response and butanone concentration. Reproduced with permission from Ref. [96] for (a–c), © Elsevier Ltd. 2021; Ref. [98] for (d–f), © Changchun Institute of Applied Chemistry, CAS 2021.

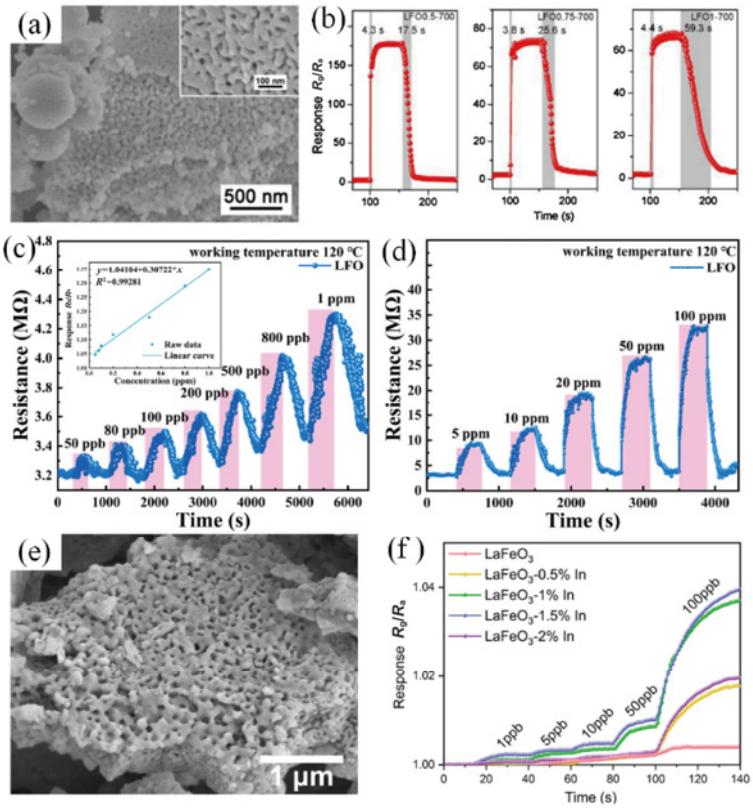

Fig. 7 (a) FESEM images of $LaFeO_3$. (b) Response/recovery curves of sensors based on 100 ppm formaldehyde at the optimal operating temperature for different $LaFeO_3$ samples. (c, d) Dynamic response curves of $LaFeO_3$ thin film gas sensors toward 0.05–100 ppm. The inset of (c) is the linear fitting curve of gas sensor toward 0.05–1 ppm formaldehyde. (e) SEM image of In-doped $LaFeO_3$. (f) Dynamic response curves of In-doped $LaFeO_3$ to 1–100 ppb. Reproduced with permission from Ref. [106] for (a, b), © Elsevier B.V. 2020; Ref. [99] for (c, d), © Elsevier B.V. 2021; Ref. [102] for (e, f), © Elsevier B.V. 2022.

short response/recovery time (3.8 s/17.5 s), high response to 50 ppb–1 ppm formaldehyde, and a low detection limit of 50 ppb at 120 ℃. In order to meet the respiratory diagnostic requirements, the detection limit should be lower than 40 ppb. Xiao *et al*. [102] improved the sensitivity to formaldehyde by doping $LaFeO_3$ with In, and the morphology of particles is shown in the Fig. 7(e). The addition of In makes the response value of In-doped $LaFeO_3$ to formaldehyde twice that of pure $LaFeO_3$ and allows the detection limit reaching 1 ppb at 122 ℃, as displayed in Fig. 7(f). These results indicate that multilayer porous $LaFeO_3$ is promising for the detection of formaldehyde of LC VOCs.

Researchers have also designed many other formaldehyde gas sensors with excellent performance. For example, CuO sensing materials with different morphologies (hierarchical flower [107] and nanotubes [108]) have high response to formaldehyde at 250–300 ℃. The CuO nanotubes prepared by Park *et al*. [108] based on the polyol process showed good selectivity to formaldehyde in the common environment VOCs at 300 ℃. In addition, the detection limit of 6 ppb at 250 ℃ can well meet the requirements of formaldehyde detection in exhaled gas. Li *et al*. [103] prepared a sensor with dual selectivity for detecting formaldehyde and acetone by modifying bimetal Pd and Au on the surface of SnO_2 nanosheets. Its detection limits for formaldehyde and acetone are 45 and 30 ppb, respectively. The sensing properties including response and selectivity are displayed in Figs. 8(a) and 8(b), respectively.

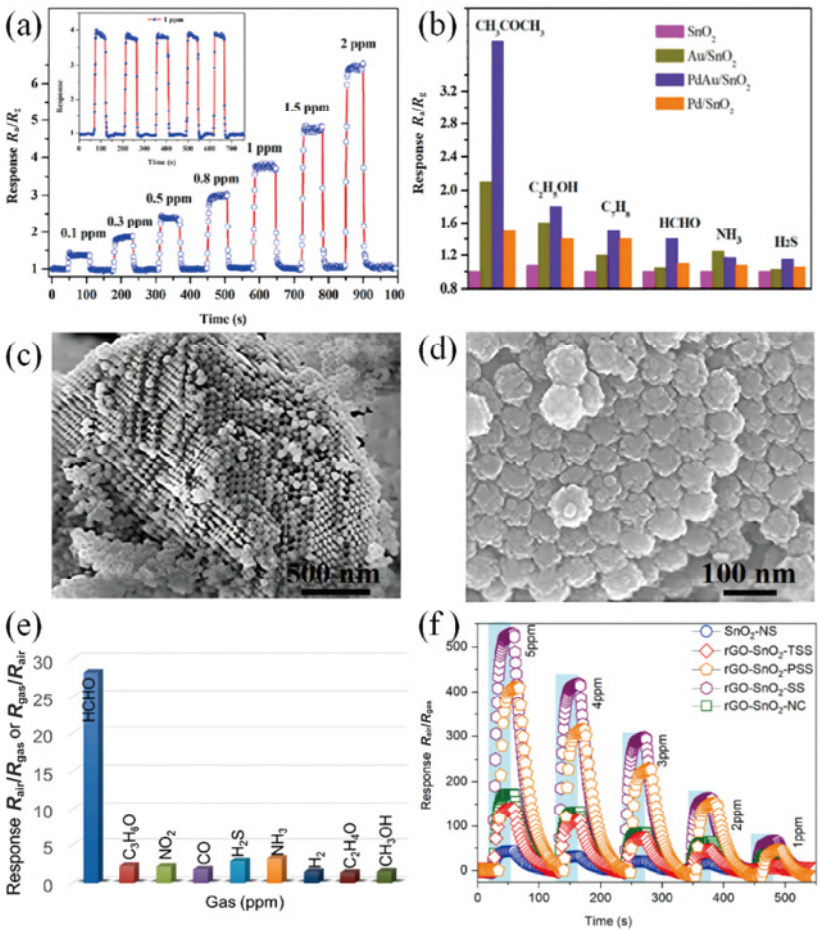

Fig. 8 (a) Representative dynamic response of Pd/Au–SnO_2 sensor to low acetone concentrations (0.1–2 ppm) at 250 ℃. The inset is five periods of response curve of Pd/Au–SnO_2 sensor to 1 ppm formaldehyde. (b) Response toward 1 ppm formaldehyde compared to 1 ppm other common interfered biomarker gases. (c, d) SEM and transmission electron microscopy (TEM) images of the prepared 3D rGO–SnO_2–SS, respectively. (e) Selectivity of the fabricated rGO–SnO_2–SS sensor toward 500 ppb formaldehyde and 1 ppm other interfering gases. (f) Dynamic sensing response characteristics of different SnO_2 sensors as a function of formaldehyde concentration (range = 1–5 ppm) at 125 ℃. Reproduced with permission from Ref. [103] for (a, b), © Elsevier B.V. 2018; Ref. [34] for (c–f), © Elsevier B.V. 2022.

Shanmugasundaram *et al*. [34] reported a 3D rGO–SnO_2 nanosphere super-structural e-nose utilized for LC detection. As displayed in Figs. 8(c) and 8(d), the morphology of 3D rGO–SnO_2–SS exhibits a honeycomb structure, which consists of uniform particles arranged regularly. The fabricated formaldehyde sensor has a detection limit of 10 ppb, high response to formaldehyde from 1 to 5 ppm, and good selectivity to formaldehyde in a variety of interfering gases at 125 ℃ (Figs. 8(e) and 8(f)). The evaluation results of this sensor for diagnosing LC showed that it can accurately distinguish between healthy and unhealthy exhaled gas. Table 2 summarizes the sensor parameters mentioned above.

3.1.5 Other VOC biomarkers for LC diagnosis

Other VOC biomarkers for LC include styrene, acetaldehyde, n-decane, and isoprene. Increased acetaldehyde levels in LC patients may result from increased membrane lipid oxidation caused by many free radicals in tumor cells. The formation mechanism of styrene, n-decane, and isoprene in LC patients is still unclear. In general, the concentration of these VOCs in the exhaled breath of LC patients is 10–100 ppb, which is higher than that of healthy people (about 1–20 ppb). The development of chemical VOC gas sensors with excellent performance is a promising strategy for LC diagnosis because of its patient-friendly characteristics. Up to now, a large number of clinical studies on respiratory LC diagnosis based on metal oxide gas sensor arrays have been carried out. Section 3.2 will summarize the gas sensor array system (including e-nose) for non-invasive LC diagnosis in detail.

3.2 Integrated gas sensor arrays for LC diagnosis

The types and concentrations of LC markers were different in almost every published study, and even the same gas showed inconsistent results in some studies. It can be explained by the lack of unified standard for respiratory detection techniques and sampling methods. A person's living environment as well as certain personal habits can also have an effect on the chemical

Table 2 Comparison of gas-sensing characteristics of sensing materials reported in the literature

Material	Structure	Target gas	Operating temperature (℃)	Detection limit	Response	Response/ recovery time (s)	Ref.
Fe-doped ZnO	Nanoneedles	Isopropanol	275	250 ppb	4.7–250 ppb	51/762	[13]
ZnO	Nanoparticle	n-propanol	125	—	6.6–40 ppm	190/200	[75]
Cu_2O	Double-shell nano hollow microspheres	n-propanol	187	10 ppm	11–100 ppm	—	[76]
$ZnSnO_3$	Nanospheres	n-propanol	200	500 ppb	1.7–500 ppb	—	[77]
NiO	Porous nanoparticles	n-propanol	75	20 ppb	1.59–20 ppb	—	[78]
ZnO/NiO	Bi-metal organic framework (MOF)	n-propanol	275	200 ppb	2.51–200 ppb	—	[79]
SnO_2	Egg yolk–shell	Toluene	250	2 ppm	20–28.6 ppm	1.8/4.1	[87]
SnO_2	Three-layer hollow cubic	Toluene	250	—	20–38.7 ppm	0.8/6.1	[88]
Pd-loaded SnO_2	Single-layer hollow cubic	Toluene	230	100 ppb	20–41.4 ppm	0.4/16.5	[89]
$NiFe_2O_4$	Ordered mesoporous structure	Toluene	230	2 ppb	1–77.3 ppm or 0.44–2 ppb	704/1523	[29]
Ce-doped SnO_2	Cuboid	Butanone	175	500 ppb	20–23.9 ppm	20/—	[94]
Ce-doped SnO_2	Thin film	Butanone	210	—	100–181 ppm	—	[95]
WO_3	Urchin	Butanone	240	100 ppb	50–188.5 ppm	7/13	[96]
Ag-modified NiO	Porous spherical	Butanone	320	50 ppb	3.2–100 ppb	5.5/8	[98]
In-doped $LaFeO_3$	Multilayer porous	Formaldehyde	125	1 ppb	100–122 ppm	36/40	[102]
3D rGO–SnO_2	Honeycomb	Formaldehyde	125	10 ppb	1–28 ppm	30/60	[34]
SnO_2 and α-Fe_2O_3 with loaded Pt	Hollow nanospheres	Styrene	206	50 ppb	10–10.56 ppm	3/15	[61]
$NiTiO_3$	Nanoparticles	Acetaldehyde	575	200 ppb	43–50 ppm	10/26	[109]
In_2O_3	Nanosheets	Isoprene	200	5 ppb	5–103.5 ppm	124/204	[110]

makeup of their exhaled. Besides, the number of the tested samples in these studies is insufficient to provide a comprehensive analysis. All these factors contribute to the fact that there are no clear VOC biomarkers for breath analysis, which are obstacles to the application of single metal oxide gas sensor-based respiratory diagnosis. A comprehensive research topic, VOC analysis for early LC detection based on semiconductor gas sensor arrays, is presented in Table 3, along with the recent studies.

As we can see, the studies of LC diagnosis based on metal oxide gas sensor arrays are well underway. Gas sensor arrays with highly integrated characteristics have been applied to establish characteristic response curves of LC VOCs, which can simultaneously analyze a variety of LC biomarkers in real time. Their remarkable achievements have significantly verified the feasibility of metal oxide gas sensor arrays in LC breath analysis. First, some gas sensor arrays have achieved relatively good accuracy, sensitivity, and specificity (over 90%) in Refs. [111,112,114]. However, some research results were not satisfactory. Some e-nose systems, made of seven metal oxide gas sensors, had accuracy and specificity of only 75% and 72%, respectively [113]. Secondly, we notice that the sensors used in most of the studies were generic metal oxide gas sensors that were already commercially available. The advantages of using general-purpose sensors are that their performance is fully explored, stable, cheap, and easy to purchase, but the disadvantages are also obvious. They usually have good sensing properties for several VOCs, work at high temperatures, and have a

Table 3 Recent studies of metal oxide gas sensor-based LC diagnosis

Author (year)	Method and technique used	Advantage	Disadvantage	Ref.
Salimi and Hosseini (2021)	• Sensor array system with 19 commercial metal oxide gas sensors	• 87 subjects were included in the experiment • The classification of data was more detailed	• Large amount of data processing • The test process took a long time	[31]
Di Gilio *et al*. (2020)	• e-nose with 10 gas sensors for breath detection • Feature extraction algorithms used PCA classifier	• Large number of LC patients (115) and healthy controls (153) were selected for the study with good accuracy	• Sensitivity and specificity are not mentioned	[26]
Chen *et al*. (2020)	• e-nose was constructed by metal-ion-induced assembly of graphene oxide • Feature extraction algorithms used PCA classifier	• Better sensitivity and specificity of 95.8% and 96%, respectively • Economical and low power consumption sensor array	• Only four VOCs were mainly analyzed, namely acetone, isoprene, hydrothion, and ammonia	[111]
Kononov *et al*. (2019)	• Sensor array system with six metal oxide chemoresistance gas sensors • Classifier-used k-nearest neighbor (k-NN), logistic regression, and linear discriminant analysis (LDA)	• The solid-state sensors keep the sensors stable for long time • Sensitivity, specificity, and accuracy of 95%, 100%, and 97.2%, respectively	• The details about current smokers, past smokers, and nonsmokers are not given • Unreasonable control group selection	[112]
Chang *et al*. (2018)	• e-nose with seven metal oxide semiconductor gas sensors for breath detection • Used LDA	• Low cost • 85 subject samples were selected	• Accuracy, sensitivity, and specificity are only 75%, 79%, and 72%, respectively • Smokers were not selected	[113]
Masuda *et al*. (2015)	• LC diagnosis system based on self-made SnO_2 nanosheet combined with SnO_2 nanoparticles and noble metal catalysts	• The functional sensor system showed an excellent detection limit of 1-nonanal, an LC biomarker	• Only 1-nonanal is tested • Still in the sensor development stage	[47]
Zhang *et al*. (2017)	• e-nose with 14 gas sensors for breath detection (including metal oxide gas sensors) • Feature extraction algorithms used LDA classifier and fuzzy k-NN	• Sensitivity, specificity, and accuracy of 91.58%, 91.72%, and 91.59%, respectively	• Only 37 subjects were included for the study	[40]
Itoh *et al*. (2016)	• Combined SnO_2-based metal oxide metal gas sensor with GC	• Gas sensor only needs to detect the concentration of a certain VOC • Good analytical capability • Enough testing samples	• Cumbersome and high cost	[46]
Güntner *et al*. (2016)	• Sensor array with four nanostructured and highly porous Pt-, Si-, Pd-, and Ti-doped SnO_2 sensing films by FSP	• Stability, high selectivity, low detection limit, and average error	• No further development and testing results	[33]
Blatt *et al*. (2007)	• Sensor array system with six highly sensitive metal oxide gas sensors (fabricated by SACMI S.C.) and fuzzy k-NN and genetic algorithm	• Low cost, small size, and short response • Accuracy, sensitivity, and specificity of over 90%	• No external factors such as smoking were considered	[18]

ppm-level detection limit. These factors indicated that the commercial sensors were not enough to detect low concentrations of specific gases in the LC breath analysis scenario. Ultimately, researchers have to rely on increasing the number of sensors and sophisticated data algorithms to increase the accuracy of the final diagnostic. Liu *et al*. [22] invented an e-nose system with high accuracy, which is an array consisting of 19 sensors. How to choose sensors and deal with the vast amount of data appropriately were systematic processes. Any data loss can directly lead to completely different results, making each sensor critical. To ensure the accuracy of diagnostic results, a series of pretreatment works (e.g., exhaled gas collection, preconcentration, dehumidification and flow control, etc.) are necessary when the existing gas sensor performance cannot meet the requirements.

In order to simplify test equipment and improve reliability, there is an urgent need for the improvement in gas-sensitive materials and preprocessing equipment to achieve rapid and portable LC diagnosis. Itoh *et al*. [46] used metal oxide sensor combined with a GC to realize the exhaled breath monitoring. GC assumed the role of identifying and separating different VOCs, and the sensor was only used for measuring the VOC concentration. The advantage of this method was that the GC system can easily solve the selectivity issue of metal oxide sensor, which can reduce the sensor effort but have good results at the same time, which offers detection capabilities comparable to those of GC–MS as they claimed. The prototype system, by contrast, did not require complex algorithms, which significantly reduced the difficulty. However, the addition of GC makes this system more expensive than those of other studies, and the system was not portable. The metal oxide gas sensors developed for LC need to perform better than general sensors, including sensitivity, selectivity, response rate, and stability. Kononov *et al*. [112] made a sensor array containing six different metal oxide gas sensors. The six sensors were all based on SnO_2 and modified with Pt, Pd, and La_2O_3, and they were sensitive to different gas compounds. They innovated an array system in three temperature regimes, allowing different sensors to work in the best condition, bringing significant performance (sensitivity = 95%, specificity = 100.0%, and accuracy = 97.2%). These results demonstrated the applicability of the e-nose for LC analysis.

3. 3 Self-powered gas sensors for breath analysis

In the past few years, Duan *et al*. [115,116] have tried to combine piezoelectric or triboelectric nanogenerator (TENG) technologies with gas sensors in an attempt to reduce the dependence on external energy sources and enhance the gas sensitivity of gas sensors. Piezoelectric nanogenerator (PENG) and TENG technologies can effectively capture and use the smallest energy sources in our lives. Under certain circumstances, self-generating technology can provide sustainable power for sensor systems, which has great application potential in the field of health detection. Due to the outstanding potential application value, sensors based on PENGs are also widely studied for the detection of various VOCs. ZnO nanowires, CdS nanorods, CuO/ZnO nanoarray-based PENGs, and Au–$MoSe_2$ nanoflowers, designed by Xue *et al*. [117], Wang *et al*. [118], Nie *et al*. [119], and Zhang *et al*. [120], respectively, have been successfully applied in self-powered gas sensor systems that can work in room temperature. However, most of them are not yet available for breath analysis at present due to the detection limits (beyond 100 ppm).

TENGs based on chitosan (CTS)/ZnO bilayer film and SnO_2-doped polyethyleneimine membrane have been successfully applied to self-powered acetone sensors that can work in high humidity environment [121,122]. However, the acetone detection limit of these self-powered sensors is usually over 1 ppm, and the response is tiny, which is not yet a good device for LC VOC diagnosing. Wang *et al*. [123] designed a breath-driven TENG–NH_3 sensor based on Ce-doped ZnO–PANI, exhibiting an excellent gas sensitivity (0.1–1 ppm), an excellent ability for identification of breathing recognition and outstanding long-term stability. Wang *et al*. [124] fabricated a NH_3 sensor based on PANI–multi-walled CNTs (MWCNTs) and high-performance TENG, exhibiting a response of 10% to 10 ppb NH_3, which proves the great application potential of TENG in disease diagnosis. However, self-powered gas sensor for breath analysis still needs to be further enhanced in many aspects, such as sensitivity, limit of detection, stability, and response time, to meet the requirements of LC VOC diagnosis.

4 Conclusions and outlook

This review has summarized recent achievements in

metal oxide materials and gas sensors applied to realize non-invasive LC diagnosis, including the mechanism of metal oxide gas sensor in LC diagnosis, specially designed metal oxide materials used for different LC VOC detection, results of sensor arrays in clinical LC diagnosis test, and breath analysis techniques based on self-powered nanogenerator. Gas sensors for LC diagnosis are evolving towards flexibility and comprehensiveness. In order to achieve a more accurate diagnosis of LC, various types of metal oxide materials were used for the exploration of LC biomarkers, and their cost-effectiveness, integration, ease of operation, non-invasiveness, rapid analysis, and portability make them appealing for LC screening and diagnosis. Due to the patient-friendly properties, metal oxide gas sensors with excellent performance should be one of the research hotspots in the future LC diagnosis.

The sensor performance and the biomarkers of LC limit their application to LC diagnosis. Although several studies on the types and concentrations of gases relevant to LC diagnosis have been published, there are currently no uniform standards. Good detection results have been obtained using e-nose and algorithms made up of different sensors, while these results are dependent on accurate data from each sensor. High-performance metal oxide gas sensors can reduce design and manufacturing difficulties of e-nose, simplify algorithms, and lower costs. In addition, to ensure diagnostic accuracy, various sensor arrays for LC VOC detection are usually accompanied by GC–MS analysis.

Although the materials mentioned in this article are excellent, LC diagnosis based on metal oxide gas sensors still faces a series of challenges. In order to reduce the influence of humidity and various interference VOCs from exhaled gas, metal oxide materials and gas sensor array systems should meet the following requirements in the future.

(1) Excellent response and selectivity toward trace-level LC VOCs.

(2) Gas sensing performance should be tiny affected by high humidity changes.

(3) Real-time response and recovery time.

(4) Long-term stability and repeatability.

With the development of stable and high-performance sensor technologies, the future direction of LC diagnosis will be modular, miniaturized, and energy efficient. So far as to meet the specific needs of different diseases or even specific individuals, researchers can choose the appropriate sensor each time. Once successfully implemented, metal oxide gas sensor-based respiratory diagnosis of LC will be of great importance to global healthcare and public health.

Acknowledgements

This work is supported by the Outstanding Youth Foundation of Jiangsu Province of China under Grant No. BK20211548, the National Natural Science Foundation of China under Grant No. 51872254, the Yangzhou City–Yangzhou University Cooperation Foundation under Grant No. YZ2021153, and the Walloon Region of Belgium through the Interreg V France–Wallonie–Vlaanderen program under PATHACOV project (Grant No. 1.1.297).

References

[1] Torre LA, Bray F, Siegel RL, *et al*. Global cancer statistics, 2012. *CA-Cancer J Clin* 2015, **65**: 87–108.

[2] Tanoue LT, Tanner NT, Gould MK, *et al*. Lung cancer screening. *Am J Resp Crit Care* 2015, **191**: 19–33.

[3] Reddy C, Chilla D, Boltax J. Lung cancer screening: A review of available data and current guidelines. *Hospital Practice* 2011, **39**: 107–112.

[4] Yorifuji T, Kashima S. Air pollution: Another cause of lung cancer. *Lancet Oncol* 2013, **14**: 788–789.

[5] Deng XB, Zhang F, Rui W, *et al*. $PM_{2.5}$-induced oxidative stress triggers autophagy in human lung epithelial A549 cells. *Toxicol in Vitro* 2013, **27**: 1762–1770.

[6] Cheema PK, Rothenstein J, Melosky B, *et al*. Perspectives on treatment advances for stage III locally advanced unresectable non-small-cell lung cancer. *Curr Oncol* 2019, **26**: 37–42.

[7] Khatoon Z, Fouad H, Alothman OY, *et al*. Doped SnO_2 nanomaterials for e-nose based electrochemical sensing of biomarkers of lung cancer. *ACS Omega* 2020, **5**: 27645–27654.

[8] Mirzaei A, Leonardi SG, Neri G. Detection of hazardous volatile organic compounds (VOCs) by metal oxide nanostructures-based gas sensors: A review. *Ceram Int* 2016, **42**: 15119–15141.

[9] Pauling L, Robinson AB, Teranishi R, *et al*. Quantitative analysis of urine vapor and breath by gas-liquid partition chromatography. *PNAS* 1971, **68**: 2374–2376.

[10] Hakim M, Broza YY, Barash O, *et al*. Volatile organic compounds of lung cancer and possible biochemical pathways. *Chem Rev* 2012, **112**: 5949–5966.

[11] Kourlaba G, Gkiozos I, Kokkotou E, *et al*. Lung cancer patients' journey from first symptom to treatment:

Results from a Greek registry. *Cancer Epidemiol* 2019, **60**: 193– 200.

[12] Adiguzel Y, Kulah H. Breath sensors for lung cancer diagnosis. *Biosens Bioelectron* 2015, **65**: 121–138.

[13] Luo YF, Ly A, Lahem D, *et al*. A novel low-concentration isopropanol gas sensor based on Fe-doped ZnO nanoneedles and its gas sensing mechanism. *J Mater Sci* 2021, **56**: 3230–3245.

[14] Zhou JM, Huang ZA, Kumar U, *et al*. Review of recent developments in determining volatile organic compounds in exhaled breath as biomarkers for lung cancer diagnosis. *Anal Chim Acta* 2017, **996**: 1–9.

[15] Thriumani R, Zakaria A, Jeffree AI, *et al*. A study on VOCs released by lung cancer cell line using GCMS–SPME. *Procedia Chem* 2016, **20**: 1–7.

[16] Liu KW, Zhang C. Volatile organic compounds gas sensor based on quartz crystal microbalance for fruit freshness detection: A review. *Food Chem* 2021, **334**: 127615.

[17] Seiyama T, Kato A, Fujiishi K, *et al*. A new detector for gaseous components using semiconductive thin films. *Anal Chem* 1962, **34**: 1502–1503.

[18] Blatt R, Bonarini A, Calabró E, *et al*. Fuzzy k-NN lung cancer identification by an electronic nose. In: *Applications of Fuzzy Sets Theory*. Francesco M, Sushmita M, Gabriella P, Eds. Berlin, Germany: Springer Berlin Heidelberg, 2007: 261–268.

[19] Uddin ASMI, Phan DT, Chung GS. Low temperature acetylene gas sensor based on Ag nanoparticles-loaded ZnO-reduced graphene oxide hybrid. *Sens Actuat B-Chem* 2015, **207**: 362–369.

[20] Li Y, Lu YL, Wu KD, *et al*. Microwave-assisted hydrothermal synthesis of copper oxide-based gas-sensitive nanostructures. *Rare Metal* 2021, **40**: 1477–1493.

[21] Binson VA, Subramoniam M. Artificial Intelligence based breath analysis system for the diagnosis of lung cancer. *J Phys Conf Ser* 2021, **1950**: 012065.

[22] Liu B, Yu HQ, Zeng XP, *et al*. Lung cancer detection via breath by electronic nose enhanced with a sparse group feature selection approach. *Sens Actuat B-Chem* 2021, **339**: 129896.

[23] Qiang Z, Ma SY, Jiao HY, *et al*. Highly sensitive and selective ethanol sensors using porous SnO_2 hollow spheres. *Ceram Int* 2016, **42**: 18983–18990.

[24] Karmaoui M, Leonardi SG, Latino M, *et al*. Pt-decorated In_2O_3 nanoparticles and their ability as a highly sensitive (< 10 ppb) acetone sensor for biomedical applications. *Sens Actuat B-Chem* 2016, **230**: 697–705.

[25] Hsu NS, Tehei M, Hossain MS, *et al*. Oxi-redox selective breast cancer treatment: An *in vitro* study of theranostic In-based oxide nanoparticles for controlled generation or prevention of oxidative stress. *ACS Appl Mater Inter* 2021, **13**: 2204–2217.

[26] Di Gilio A, Catino A, Lombardi A, *et al*. Breath analysis for early detection of malignant pleural mesothelioma: Volatile organic compounds (VOCs) determination and possible biochemical pathways. *Cancers* 2020, **12**: 1262.

[27] Haick H, Broza YY, Mochalski P, *et al*. Assessment, origin, and implementation of breath volatile cancer markers. *Chem Soc Rev* 2014, **43**: 1423–1449.

[28] Gregis G, Sanchez JB, Bezverkhyy I, *et al*. Detection and quantification of lung cancer biomarkers by a micro-analytical device using a single metal oxide-based gas sensor. *Sens Actuat B-Chem* 2018, **255**: 391–400.

[29] Lai XY, Cao K, Shen GX, *et al*. Ordered mesoporous $NiFe_2O_4$ with ultrathin framework for low-ppb toluene sensing. *Sci Bull* 2018, **63**: 187–193.

[30] Luo YF, Ly A, Lahem D, *et al*. Role of cobalt in Co–ZnO nanoflower gas sensors for the detection of low concentration of VOCs. *Sens Actuat B-Chem* 2022, **360**: 131674.

[31] Salimi M, Hosseini SMRM. Smartphone-based detection of lung cancer-related volatile organic compounds (VOCs) using rapid synthesized ZnO nanosheet. *Sens Actuat B-Chem* 2021, **344**: 130127.

[32] Hermawan A, Amrillah T, Riapanitra A, *et al*. Prospects and challenges of MXenes as emerging sensing materials for flexible and wearable breath-based biomarker diagnosis. *Adv Healthc Mater* 2021, **10**: 2100970.

[33] Güntner AT, Koren V, Chikkadi K, *et al*. E-nose sensing of low-ppb formaldehyde in gas mixtures at high relative humidity for breath screening of lung cancer? *ACS Sens* 2016, **1**: 528–535.

[34] Shanmugasundaram A, Manorama SV, Kim DS, *et al*. Toward point-of-care chronic disease management: Biomarker detection in exhaled breath using an e-nose sensor based on rGO/SnO_2 superstructures. *Chem Eng J* 2022, **448**: 137736.

[35] Fu XA, Li MX, Knipp RJ, *et al*. Noninvasive detection of lung cancer using exhaled breath. *Cancer Med* 2014, **3**: 174–181.

[36] Ma W, Gao P, Fan J, *et al*. Determination of breath gas composition of lung cancer patients using gas chromatography/mass spectrometry with monolithic material sorptive extraction. *Biomed Chromatogr* 2015, **29**: 961–965.

[37] Hu J, Xiong XQ, Guan WW, *et al*. Self-templated flower-like WO_3–In_2O_3 hollow microspheres for conductometric acetone sensors. *Sens Actuat B-Chem* 2022, **361**: 131705.

[38] Lee J, Choi Y, Park BJ, *et al*. Precise control of surface oxygen vacancies in ZnO nanoparticles for extremely high acetone sensing response. *J Adv Ceram* 2022, **11**: 769–783.

[39] Liu D, Ren XW, Li YS, *et al*. Nanowires-assembled WO_3 nanomesh for fast detection of ppb-level NO_2 at low temperature. *J Adv Ceram* 2020, **9**: 17–26.

[40] Zhang K, Yang X, Wang YZ, *et al*. Pd-loaded SnO_2 ultrathin nanorod-assembled hollow microspheres with the significant improvement for toluene detection. *Sens Actuat B-Chem* 2017, **243**: 465–474.

[41] Samadi S, Nouroozshad M, Zakaria SA. ZnO@SiO_2/rGO core/shell nanocomposite: A superior sensitive, selective

and reproducible performance for 1-propanol gas sensor at room temperature. *Mater Chem Phys* 2021, **271**: 124884.

[42] Zhang C, Huan YC, Li Y, *et al*. Low concentration isopropanol gas sensing properties of Ag nanoparticles decorated In_2O_3 hollow spheres. *J Adv Ceram* 2022, **11**: 379–391.

[43] Kim HJ, Lee JH. Highly sensitive and selective gas sensors using p-type oxide semiconductors: Overview. *Sens Actuat B-Chem* 2014, **192**: 607–627.

[44] Xu JY, Zhang C. Oxygen vacancy engineering on cerium oxide nanowires for room-temperature linalool detection in rice aging. *J Adv Ceram* 2022, **11**: 1559–1570.

[45] Marzorati D, Mainardi L, Sedda G, *et al*. MOS sensors array for the discrimination of lung cancer and at-risk subjects with exhaled breath analysis. *Chemosensors* 2021, **9**: 209.

[46] Itoh T, Miwa T, Tsuruta A, *et al*. Development of an exhaled breath monitoring system with semiconductive gas sensors, a gas condenser unit, and gas chromatograph columns. *Sensors* 2016, **16**: 1891.

[47] Masuda Y, Itoh T, Shin W, *et al*. SnO_2 nanosheet/nanoparticle detector for the sensing of 1-nonanal gas produced by lung cancer. *Sci Rep* 2015, **5**: 10122.

[48] Hsu KC, Fang TH, Chen SH, *et al*. Gas sensitivity and sensing mechanism studies on ZnO/$La_{0.8}Sr_{0.2}Co_{0.5}Ni_{0.5}O_3$ heterojunction structure. *Ceram Int* 2019, **45**: 8744–8749.

[49] Lv L, Cheng PF, Wang YL, *et al*. Sb-doped three-dimensional $ZnFe_2O_4$ macroporous spheres for *N*-butanol chemiresistive gas sensors. *Sens Actuat B-Chem* 2020, **320**: 128384.

[50] Zhang C, Wu QD, Zheng BB, *et al*. Synthesis and acetone gas sensing properties of Ag activated hollow sphere structured $ZnFe_2O_4$. *Ceram Int* 2018, **44**: 20700–20707.

[51] Guo WW, Huang LL, Liu XC, *et al*. Enhanced isoprene gas sensing performance based on p-$CaFe_2O_4$/n-$ZnFe_2O_4$ heterojunction composites. *Sens Actuat B-Chem* 2022, **354**: 131243.

[52] Smiy S, Bejar M, Dhahri E, *et al*. Ozone detection based on nanostructured $La_{0.8}Pb_{0.1}Ca_{0.1}Fe_{0.8}Co_{0.2}O_3$ thin films. *J Alloys Compd* 2020, **829**: 154596.

[53] Kumar D, Chaturvedi P, Saho P, *et al*. Effect of single wall carbon nanotube networks on gas sensor response and detection limit. *Sens Actuat B-Chem* 2017, **240**: 1134–1140.

[54] Zhang XX, Cui H, Gui YG, *et al*. Mechanism and application of carbon nanotube sensors in SF_6 decomposed production detection: A review. *Nanoscale Res Lett* 2017, **12**: 177.

[55] Lee SW, Lee W, Hong Y, *et al*. Recent advances in carbon material-based NO_2 gas sensors. *Sens Actuat B-Chem* 2018, **255**: 1788–1804.

[56] Freddi S, Emelianov AV, Bobrinetskiy II, *et al*. Development of a sensing array for human breath analysis based on SWCNT layers functionalized with semiconductor organic molecules. *Adv Healthc Mater* 2020, **9**: 2000377.

[57] Inaba M, Oda T, Kono M, *et al*. Effect of mixing ratio on NO_2 gas sensor response with SnO_2-decorated carbon nanotube channels fabricated by one-step dielectrophoretic assembly. *Sens Actuat B-Chem* 2021, **344**: 130257.

[58] Zhang J, Liu XH, Neri G, *et al*. Nanostructured materials for room-temperature gas sensors. *Adv Mater* 2016, **28**: 795–831.

[59] Mansha M, Qurashi A, Ullah N, *et al*. Synthesis of In_2O_3/graphene heterostructure and their hydrogen gas sensing properties. *Ceram Int* 2016, **42**: 11490–11495.

[60] Soleymaniha M, Shahbazi MA, Rafieerad AR, *et al*. Promoting role of MXene nanosheets in biomedical sciences: Therapeutic and biosensing innovations. *Adv Healthc Mater* 2019, **8**: 1801137.

[61] Liu B, Li YY, Gao L, *et al*. Ultrafine Pt NPs-decorated SnO_2/α-Fe_2O_3 hollow nanospheres with highly enhanced sensing performances for styrene. *J Hazard Mater* 2018, **358**: 355–365.

[62] Zhou MZ, Liu YC, Su Y, *et al*. Plasmonic oxygen defects in MO_{3-x} (M = W or Mo) nanomaterials: Synthesis, modifications, and biomedical applications. *Adv Healthc Mater* 2021, **10**: 2101331.

[63] Zhou AG, Liu Y, Li SB, *et al*. From structural ceramics to 2D materials with multi-applications: A review on the development from MAX phases to MXenes. *J Adv Ceram* 2021, **10**: 1194–1242.

[64] Zheng ZX, Wu W, Yang T, *et al*. *In situ* reduced MXene/AuNPs composite toward enhanced charging/discharging and specific capacitance. *J Adv Ceram* 2021, **10**: 1061–1071.

[65] Kim Y, Lee S, Song JG, *et al*. 2D transition metal dichalcogenide heterostructures for p- and n-type photovoltaic self-powered gas sensor. *Adv Funct Mater* 2020, **30**: 2003360.

[66] Wang S, Jiang YD, Liu BH, *et al*. Ultrathin Nb_2CT_x nanosheets-supported polyaniline nanocomposite: Enabling ultrasensitive NH_3 detection. *Sens Actuat B-Chem* 2021, **343**: 130069.

[67] Hermawan A, Zhang B, Taufik A, *et al*. CuO nanoparticles/$Ti_3C_2T_x$ MXene hybrid nanocomposites for detection of toluene gas. *ACS Appl Nano Mater* 2020, **3**: 4755–4766.

[68] Umar A, Ibrahim AA, Algadi H, *et al*. Enhanced NO_2 gas sensor device based on supramolecularly assembled polyaniline/silver oxide/graphene oxide composites. *Ceram Int* 2021, **47**: 25696–25707.

[69] Duan XH, Duan ZH, Zhang YJ, *et al*. Enhanced NH_3 sensing performance of polyaniline via a facile morphology modification strategy. *Sens Actuat B-Chem* 2022, **369**: 132302.

[70] Bai SL, Tian YL, Cui M, *et al*. Polyaniline@SnO_2 heterojunction loading on flexible PET thin film for detection of NH_3 at room temperature. *Sens Actuat B-Chem* 2016, **226**: 540–547.

[71] Koureas M, Kirgou P, Amoutzias G, *et al*. Target analysis

of volatile organic compounds in exhaled breath for lung cancer discrimination from other pulmonary diseases and healthy persons. *Metabolites* 2020, **10**: 317.

[72] Kim SJ, Choi SJ, Jang JS, *et al*. Mesoporous WO_3 nanofibers with protein-templated nanoscale catalysts for detection of trace biomarkers in exhaled breath. *ACS Nano* 2016, **10**: 5891–5899.

[73] Huang SP, Wang T, Xiao Q. Effect of Fe doping on the structural and gas sensing properties of ZnO porous microspheres. *J Phys Chem Solids* 2015, **76**: 51–58.

[74] Zhang Y, Han S, Wang MY, *et al*. Electrospun Cu-doped In_2O_3 hollow nanofibers with enhanced H_2S gas sensing performance. *J Adv Ceram* 2022, **11**: 427–442.

[75] Kortidis I, Lushozi S, Leshabane N, *et al*. Selective detection of propanol vapour at low operating temperature utilizing ZnO nanostructures. *Ceram Int* 2019, **45**: 16417–16423.

[76] Wang N, Zhou Y, Chen K, *et al*. Double shell Cu_2O hollow microspheres as sensing material for high performance n-propanol sensor. *Sens Actuat B-Chem* 2021, **333**: 129540.

[77] Yin YY, Shen YB, Zhou PF, *et al*. Fabrication, characterization and n-propanol sensing properties of perovskite-type $ZnSnO_3$ nanospheres based gas sensor. *Appl Surf Sci* 2020, **509**: 145335.

[78] Mokoena TP, Swart HC, Hillie KT, *et al*. Enhanced propanol gas sensing performance of p-type NiO gas sensor induced by exceptionally large surface area and crystallinity. *Appl Surf Sci* 2022, **571**: 151121.

[79] Zhao YM, Wang S, Zhai X, *et al*. Construction of Zn/Ni bimetallic organic framework derived ZnO/NiO heterostructure with superior n-propanol sensing performance. *ACS Appl Mater Inter* 2021, **13**: 9206–9215.

[80] Lei GL, Pan HY, Mei HS, *et al*. Emerging single atom catalysts in gas sensors. *Chem Soc Rev* 2022, **51**: 7260–7280.

[81] Lin CY, Wang WH, Lee CS, *et al*. Magnetophotoluminescence properties of Co-doped ZnO nanorods. *Appl Phys Lett* 2009, **94**: 151909.

[82] Zhu L, Li YQ, Zeng W. Hydrothermal synthesis of hierarchical flower-like ZnO nanostructure and its enhanced ethanol gas-sensing properties. *Appl Surf Sci* 2018, **427**: 281–287.

[83] Motaung DE, Mhlongo GH, Makgwane PR, *et al*. Ultra-high sensitive and selective H_2 gas sensor manifested by interface of n–n heterostructure of CeO_2–SnO_2 nanoparticles. *Sens Actuat B-Chem* 2018, **254**: 984–995.

[84] Chen HJ, Bo RH, Shrestha A, *et al*. NiO–ZnO nanoheterojunction networks for room-temperature volatile organic compounds sensing. *Adv Opt Mater* 2018, **6**: 1800677.

[85] Gregis G, Schaefer S, Sanchez JB, *et al*. Characterization of materials toward toluene traces detection for air quality monitoring and lung cancer diagnosis. *Mater Chem Phys* 2017, **192**: 374–382.

[86] Wang L, Song SY, Hong B, *et al*. Highly improved toluene gas-sensing performance of mesoporous Co_3O_4 nanowires and physical mechanism. *Mater Res Bull* 2021, **140**: 111329.

[87] Bing YF, Liu C, Qiao L, *et al*. Multistep synthesis of non-spherical SnO_2@SnO_2 yolk–shell cuboctahedra with nanoparticle-assembled porous structure for toluene detection. *Sens Actuat B-Chem* 2016, **231**: 365–375.

[88] Wang TY, Xu HY, Wang YZ, *et al*. Porous SnO_2 triple-shelled hollow nanoboxes for high sensitive toluene detection. *Mater Lett* 2020, **264**: 127320.

[89] Qiao L, Bing YF, Wang YZ, *et al*. Enhanced toluene sensing performances of Pd-loaded SnO_2 cubic nanocages with porous nanoparticle-assembled shells. *Sens Actuat B-Chem* 2017, **241**: 1121–1129.

[90] Saalberg Y, Wolff M. VOC breath biomarkers in lung cancer. *Clin Chim Acta* 2016, **459**: 5–9.

[91] Nasiri N, Clarke C. Nanostructured chemiresistive gas sensors for medical applications. *Sensors* 2019, **19**: 462.

[92] Buszewski B, Ligor T, Jezierski T, *et al*. Identification of volatile lung cancer markers by gas chromatography–mass spectrometry: Comparison with discrimination by canines. *Anal Bioanal Chem* 2012, **404**: 141–146.

[93] Zito CA, Perfecto TM, Oliveira TNT, *et al*. Bicone-like ZnO structure as high-performance butanone sensor. *Mater Lett* 2018, **223**: 142–145.

[94] Zhang YQ, Wang C, Zhao LJ, *et al*. Preparation of Ce-doped SnO_2 cuboids with enhanced 2-butanone sensing performance. *Sens Actuat B-Chem* 2021, **341**: 130039.

[95] Jiang ZW, Guo Z, Sun B, *et al*. Highly sensitive and selective butanone sensors based on cerium-doped SnO_2 thin films. *Sens Actuat B-Chem* 2010, **145**: 667–673.

[96] Tian YC, Xu DP, Liu C, *et al*. Sea urchin-like mesoporous WO_3 (SUS-WO_3) for sensitive 3-hydroxy-2-butanone biomarker detection. *Mater Sci Semicon Proc* 2022, **137**: 106160.

[97] Yuan ZY, Yang C, Li YD, *et al*. ppb-level 2-butanone gas sensor based on CTAB-assisted synthesis of small-size ZnSnO nano cube. *IEEE Sens J* 2022, **22**: 20156–20164.

[98] Zhu HM, Qin WB, Yuan ZY, *et al*. ppb-level butanone sensor based on porous spherical NiO and the influence of silver modification. *Chin J Anal Chem* 2022, **50**: 100034.

[99] Hu JY, Chen XQ, Zhang Y. Batch fabrication of formaldehyde sensors based on $LaFeO_3$ thin film with ppb-level detection limit. *Sens Actuat B-Chem* 2021, **349**: 130738.

[100] Fuchs P, Loeseken C, Schubert JK, *et al*. Breath gas aldehydes as biomarkers of lung cancer. *Int J Cancer* 2010, **126**: 2663–2670.

[101] Lou CM, Lei GL, Liu XH, *et al*. Design and optimization strategies of metal oxide semiconductor nanostructures for advanced formaldehyde sensors. *Coordin Chem Rev* 2022, **452**: 214280.

[102] Xiao CL, Zhang XH, Ma ZZ, *et al*. Formaldehyde gas sensor with 1 ppb detection limit based on In-doped

$LaFeO_3$ porous structure. *Sens Actuat B-Chem* 2022, **371**: 132558.

[103] Li GJ, Cheng ZX, Xiang Q, *et al*. Bimetal PdAu decorated SnO_2 nanosheets based gas sensor with temperature-dependent dual selectivity for detecting formaldehyde and acetone. *Sens Actuat B-Chem* 2019, **283**: 590–601.

[104] Niu JS, Liu IP, Pan YL, *et al*. Study of a formaldehyde gas sensor based on a sputtered vanadium pentoxide thin film decorated with gold nanoparticles. *ECS J Solid State Sc* 2021, **10**: 087001.

[105] Lou CM, Yang C, Zheng W, *et al*. Atomic layer deposition of ZnO on SnO_2 nanospheres for enhanced formaldehyde detection. *Sens Actuat B-Chem* 2021, **329**: 129218.

[106] Yang K, Ma JZ, Qiao XK, *et al*. Hierarchical porous $LaFeO_3$ nanostructure for efficient trace detection of formaldehyde. *Sens Actuat B-Chem* 2020, **313**: 128022.

[107] Deng H, Li HR, Wang F, *et al*. A high sensitive and low detection limit of formaldehyde gas sensor based on hierarchical flower-like CuO nanostructure fabricated by sol–gel method. *J Mater Sci*: *Mater Electron* 2016, **27**: 6766–6772.

[108] Park HJ, Choi NJ, Kang H, *et al*. A ppb-level formaldehyde gas sensor based on CuO nanocubes prepared using a polyol process. *Sens Actuat B-Chem* 2014, **203**: 282–288.

[109] Wang J, Jiang L, Zhao LJ, *et al*. Mixed potential type ppb-level acetaldehyde gas sensor based on stabilized zirconia electrolyte and a $NiTiO_3$ sensing electrode. *Sens Actuat B-Chem* 2020, **320**: 128329.

[110] Han BQ, Wang HR, Yang WY, *et al*. Hierarchical Pt-decorated In_2O_3 microspheres with highly enhanced isoprene sensing properties. *Ceram Int* 2021, **47**: 9477–9485.

[111] Chen QF, Chen Z, Liu D, *et al*. Constructing an E-nose using metal-ion-induced assembly of graphene oxide for diagnosis of lung cancer via exhaled breath. *ACS Appl Mater Inter* 2020, **12**: 17713–17724.

[112] Kononov A, Korotetsky B, Jahatspanian I, *et al*. Online breath analysis using metal oxide semiconductor sensors (electronic nose) for diagnosis of lung cancer. *J Breath Res* 2019, **14**: 016004.

[113] Chang JE, Lee DS, Ban SW, *et al*. Analysis of volatile organic compounds in exhaled breath for lung cancer diagnosis using a sensor system. *Sens Actuat B-Chem* 2018, **255**: 800–807.

[114] Li W, Liu HY, Xie DD, *et al*. Lung cancer screening based on type-different sensor arrays. *Sci Rep* 2017, **7**: 1969.

[115] Zhao QN, Jiang YD, Duan ZH, *et al*. A Nb_2CT_x/sodium alginate-based composite film with neuron-like network for self-powered humidity sensing. *Chem Eng J* 2022, **438**: 135588.

[116] Duan ZH, Yuan Z, Jiang YD, *et al*. Power generation humidity sensor based on primary battery structure. *Chem Eng J* 2022, **446**: 136910.

[117] Xue XY, Nie YX, He B, *et al*. Surface free-carrier screening effect on the output of a ZnO nanowire nanogenerator and its potential as a self-powered active gas sensor. *Nanotechnology* 2013, **24**: 225501.

[118] Wang PL, Deng P, Nie YX, *et al*. Synthesis of CdS nanorod arrays and their applications in flexible piezo-driven active H_2S sensors. *Nanotechnology* 2014, **25**: 075501.

[119] Nie YX, Deng P, Zhao YY, *et al*. The conversion of PN-junction influencing the piezoelectric output of a CuO/ZnO nanoarray nanogenerator and its application as a room-temperature self-powered active H_2S sensor. *Nanotechnology* 2014, **25**: 265501.

[120] Zhang DZ, Yang ZM, Li P, *et al*. Flexible self-powered high-performance ammonia sensor based on Au-decorated $MoSe_2$ nanoflowers driven by single layer MoS_2-flake piezoelectric nanogenerator. *Nano Energy* 2019, **65**: 103974.

[121] Liu BH, Libanori A, Zhou YH, *et al*. Simultaneous biomechanical and biochemical monitoring for self-powered breath analysis. *ACS Appl Mater Inter* 2022, **14**: 7301–7310.

[122] Liu BH, Wang S, Yuan Z, *et al*. Novel chitosan/ZnO bilayer film with enhanced humidity-tolerant property: Endowing triboelectric nanogenerator with acetone analysis capability. *Nano Energy* 2020, **78**: 105256.

[123] Wang S, Tai HL, Liu BH, *et al*. A facile respiration-driven triboelectric nanogenerator for multifunctional respiratory monitoring. *Nano Energy* 2019, **58**: 312–321.

[124] Wang S, Xie GZ, Tai HL, *et al*. Ultrasensitive flexible self-powered ammonia sensor based on triboelectric nanogenerator at room temperature. *Nano Energy* 2018, **51**: 231–240.